

# MILKY WAY HALO VIBRATIONS AND INCOMMENSURATE STREAM VELOCITIES

RAYMOND G. CARLBERG

Department of Astronomy & Astrophysics, University of Toronto, Toronto, ON M5S 3H4, Canada  
*Draft version February 12, 2019*

## ABSTRACT

Collisionless dark matter galactic halos are expected to exhibit damped oscillations as a result of ongoing late time accretion. An n-body model of the cosmological assembly of a Milky Way-like halo is used to quantify the time dependence of its gravitational field. The simulation contains stellar streams whose incommensurate perpendicular velocities are found to have an approximately exponential distribution with a scale of 10-20 km s<sup>-1</sup>, depending on how the stars are selected, comparable to those reported for the Orphan stream. The fluctuations in the quadrupole moment of the dark matter halo are sufficient to largely explain the tangential velocities. If velocity measurements of a larger sample of Milky Way streams finds (or does not find) the expected distribution of transverse velocities it will lead to limits on the cross-section of self-interacting dark matter, in which kinetic viscosity can damp the oscillations more rapidly than the mixing processes of collisionless dark matter alone.

*Subject headings:* dark matter; Galaxy: halo

## 1. INTRODUCTION

The gravitational force from the Milky Way's halo is conventionally and conveniently derived from a static potential (Navarro et al. 1997; Bovy 2015). However, the late time accretion of mass and the motions of satellites means that the halo potential is time variable at a level which can be important for some aspects of orbital motion. The DR2 data release (Gaia Collaboration et al. 2018) of the Gaia mission (Gaia Collaboration et al. 2016) has provided some intriguing new insight into the non-stationary aspects of the galactic potential. Within a few kiloparsecs of the sun the motion of stars led Carrillo et al. (2018) to reach the conclusion that the stellar distribution around the sun is “wobbly”, with both bending and breathing modes present, with a velocity amplitude in the range 5-10 km s<sup>-1</sup> kpc<sup>-1</sup>. Spiral waves, the galactic bar and bending waves dominate the time dependent component potential in the region near the sun (Darling & Widrow 2019) so it is unclear what variation there might be in the dark matter halo.

The stars that gravitational tides pull away from dynamically evaporating globular clusters and low mass dwarf galaxies create long thin streams of stars with a narrow range of initial velocities close to the orbit of the progenitor system. The narrow range in velocities of the stars means that streams are sensitive indicators of the galactic potential along the path of the stream. The stream path, and the underlying orbits of its constituent stars, has been extensively studied in a range of realistic potentials with powerful methods that can be adapted to almost any frozen potential (Binney 2008; Eyre & Binney 2009; Sanders & Binney 2013). Although systematic offsets between the path of the stream and the orbits of its stars are expected, the offsets of the stream velocities from the path of the stream are comparable to the range that the progenitor system introduces at the outset, typically a few km s<sup>-1</sup> for globular clusters and low mass dwarf galaxies. The stars of the Orphan stream have been found to have systematic and coherent velocities

transverse to the stream path of tens of km s<sup>-1</sup> (Koposov et al. 2018). That is, the velocities are incommensurate with the stream path, strongly suggesting that the Milky Way halo potential must have a significant time dependence. Erkal et al. (2018) shows that a model of a static halo with the approaching Large Magellanic Cloud can successfully reproduce the data.

Dark matter at the current epoch is often assumed to have a sufficiently low cross-section for interaction with itself and other particles that it is effectively collisionless. Particle dark matter at the current epoch almost certainly has a small but finite cross-section for interaction which could help with the problem of cores of dark matter halos in dwarf galaxies (Spergel & Steinhardt 2000). However the past presence of gas in dwarf cores complicates their interpretation (Harvey et al. 2018; Read et al. 2019). Locations which have plausibly never had much baryonic influence, such as the halo of the Milky Way galaxy are likely a cleaner environment to study the properties of dark matter.

The purpose of this paper is to assess the level of potential fluctuations that arise from the vibrations or ringing of a Milky Way-like dark halo due to ongoing late time mass accretion and how that affects the orbits of stellar streams. The approach is to use an n-body model of the build-up of a Milky Way model which contains globular clusters which are undergoing dynamical evaporation to produce stellar streams.

## 2. SIMULATION AND STREAMS

The simulation here is the same as used in Carlberg (2019) to create a dominant Milky Way-like halo from LCDM initial conditions. The simulation begins at redshift 3, reconstituting the halo catalog of the VL2 simulation (Madau et al. 2008). The dark matter particles have masses of  $4 \times 10^4 M_{\odot}$  and softening of 200 pc. Added to the simulation is a dynamical population of globular clusters, evolved with a softening length of 2 pc and using star particles of  $10 M_{\odot}$ . The simulation does not include any gas particles, or, the buildup of a central disk galaxy, since neither is a significant concern for the stream pop-

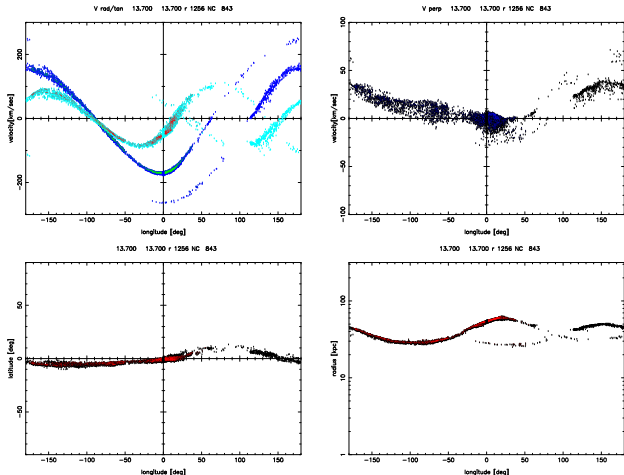


FIG. 1.— An example of a stream with significant transverse velocities. The frame is rotated to place the progenitor cluster at the origin with its velocity aligned to the left along the equator. The upper left panel shows the radial (red/cyan) and longitudinal velocities (green/blue) where the first color is for the star particles within the part of the stream that a thin stream finder identifies. The upper right panel shows the velocities perpendicular to the stream with the thin stream in blue. The lower left panel shows the stream on the sky, with the thin stream in red. The lower right shows the radial distance from the center.

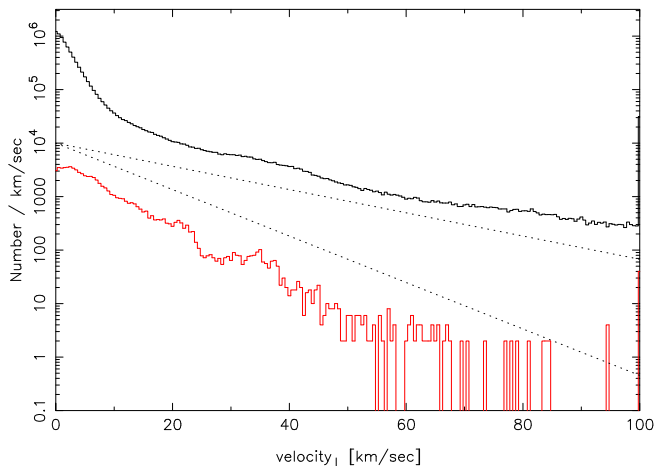


FIG. 2.— The distribution of velocities perpendicular to the streams for all stream stars in the radial range 10-70 kpc. All stream particles are shown in black and the identified thin stream particles in red. The dashed lines are exponential functions with scales of 10 and 20  $\text{km s}^{-1}$ .

ulation beyond about 30 kpc from the primary halo center. The outcome is a main galactic halo similar to the VL2 result with a low level of ongoing accretion. Pynbody (Pontzen et al. 2013) reports the instantaneous final shape of the halo to have  $(b/a, c/a)$  values of (0.95, 0.90) and (0.92, 0.83) at 27 and 41 kpc, respectively.

The inserted star clusters are drawn from a power law cluster mass distribution over the range  $2 \times 10^6 M_\odot$  to  $5 \times 10^4 M_\odot$ . In total, 1433 are clusters started. The

star particles have a mass of  $10 M_\odot$  and a softening of 2 pc. The clusters lose mass as a result of internal two body relaxation and tidal fields to produce long, thin tidal streams that have roughly the same properties as star streams found in the Milky Way. The streams are identified in the radial range of 0 to 150 kpc, which leads to 119 streams. The cluster mass loss initially takes place in their initial dark matter sub-halo which often merges into the growing dominant halo where the clusters orbit freely. The considerable number of stars lost from the star cluster while in the sub-halo are spread out in a broader distribution of width and length, reflecting the size and velocity of the cluster’s orbit in the sub-halo. The free orbit mass loss produces a stream whose width is comparable to the tidal radius of the cluster, of order 100 pc.

To analyze the properties of the stream, the star coordinates are rotated into a frame where the progenitor cluster is located at the coordinate center on the sky, with the cluster moving to the left along the equator. Figure 1 shows one stream that has properties similar to those of the Orphan stream (Belokurov et al. 2007; Newberg et al. 2010; Koposov et al. 2018). About 10% of the 119 streams have tangential velocities and other properties similar to the stream displayed in Figure 1. Many of those streams have progenitor clusters still present, however that does not effect the kinematic properties of the stream.

Figure 2 quantifies the distribution of velocities perpendicular to the velocity vector of the star cluster for stars in the radial range 10-70 kpc from all streams. That is, all streams that qualify as thin and at least  $20^\circ$  long with stars in the selected radial range are plotted. The red distribution is for stars within the thin stream and the black distribution is for all stars. The location of the two sets of stars on the sky are shown in Figure 1 in the lower left panel. Approximating the velocity distribution in the  $10\text{-}50 \text{ km s}^{-1}$  range as  $\exp(-v/v_s)$ , then  $v_s$  is approximately 10 and  $20 \text{ km s}^{-1}$  for the thin stream and all stream stars, respectively. Creating the same plot as Figure 2 at any time up to 4 Gyr earlier shows essentially the same distribution. That is, significant incommensurate velocities perpendicular to the stream path are always present at late times.

### 3. ANALYSIS OF STREAM VELOCITIES

The streams in the simulation have a range of velocities perpendicular to the stream direction, some comparable to those in the Orphan Stream. The question is what aspects of the gravitational potential give rise to those velocities. The simulations do not have a large satellite comparable to the LMC at late times. The late time accretion is fairly modest with the mass inside 100 kpc rising about 2% from 9.16 to 13.4 Gyr, with the mass inside 25 kpc constant with 0.7% variance.

A straightforward procedure to measure large scale fluctuations in the gravitational potential is to calculate the quadrupole potential as a function of radius. Because the vertical velocities vary slowly with longitude around the orbit, with one or two maxima in latitude, moments higher than the quadrupole are ignored. The quadrupole

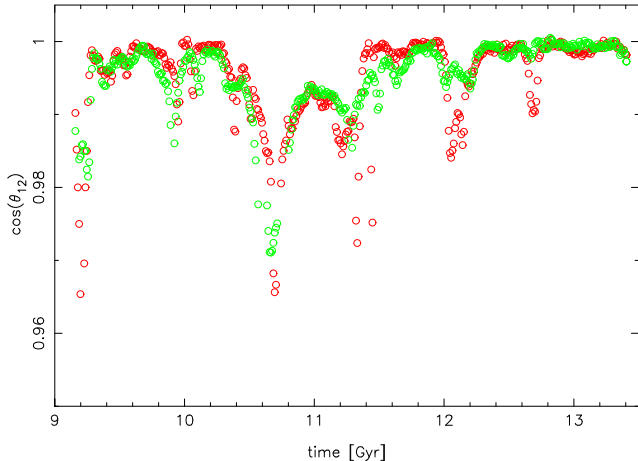


FIG. 3.— The cosine of the angle between the major axis vector at the final moment and earlier times. Red is at 25 kpc and green 32 kpc. The major axis has a nearly constant direction.

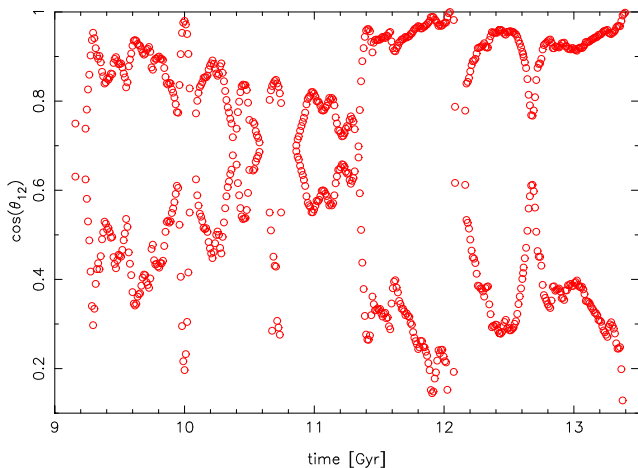


FIG. 4.— The cosine of the angle between the second largest eigenvector at the final moment and the second and third eigenvector at earlier times. The direction of the second and third eigenvector swap with each other as the halo vibrates. Starting from the final moment the alignment of the second eigenvector with itself, on the average, goes to zero at 9 Gyr. The alignment of the second eigenvector with the third eigenvector becomes stronger, on the average, to earlier times. That is, on the average, the halo quadrupole potential turns about  $90^\circ$  over this time interval.

potential is calculated as,

$$\phi_2(r') = -Gm_p \sum_{ij} \sum_m \left[ \frac{3}{2r^5} a_i a_j r_i r_j - \frac{a^2}{2r^3} \right]. \quad (1)$$

The  $ij$  sum is over coordinate directions and the  $m$  sum is over the positions of all particles of mass  $m_p$ . The  $m$  sum is over the  $a$  coordinates for  $a < r'$  with  $r = r'$ , and over  $r$  coordinates for  $r > r'$ , with  $a = r'$ . Note that only the first term generates non-radial forces. The coordinate center is defined as the location of the highest particle density. To analyze the time variability of the potential the eigenvalues and eigenvectors of the quadrupole po-

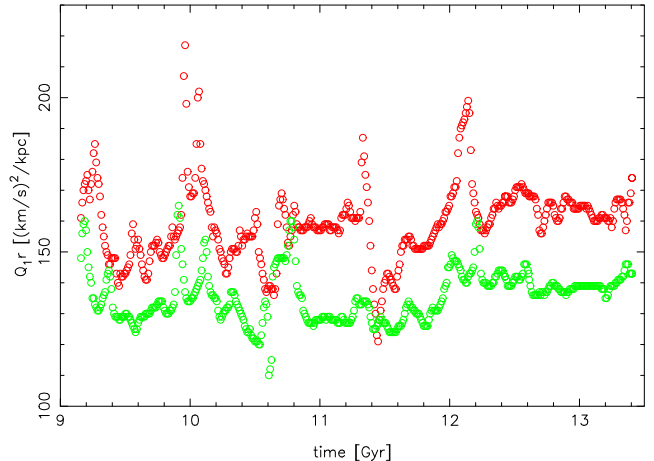


FIG. 5.— The tangential acceleration inferred from the largest eigenvalue of the quadrupole potential. Red is the analysis for 25 kpc potentials and green for 32 kpc.

tential matrix are found. The orientation of the largest eigenvector at the last moment (current epoch) of the simulation defines the reference direction. Figure 3 plots the dot product of the reference with the same vector at earlier times, finding that the orientation of the major axis varies about  $8^\circ$  over times that are comparable to the dynamical time at the two radii considered. The major axis of the halo wobbles, but not a lot.

The dot product of the eigenvector associated with the second largest eigenvalue with itself and the third axis shows a slow drift with large swings, as shown in Figure 4 with the second and third largest eigenvectors switching with each other from time to time. Using the final moment of the simulation as the reference directions, at earlier times the alignment of the second eigenvector with itself gradually goes to zero, albeit with many large fluctuations. The alignment of the third eigenvector with the late time second eigenvector gradually increases to strong alignment, again with considerable variation, and the directions of the second and third largest eigenvalues often swap. The change in angles is simply interpreted as showing a slow systematic rotation of about  $90^\circ$  over the 5 Gyr shown. The implied rotation period is then 20 some Gyr, much longer than the dynamical time of approximately 0.5 Gyr at 25 kpc, which the stars will see as a nearly adiabatic change and will not lead to significant transverse velocities.

The gravitational acceleration monopole has a mean of  $2300(\text{km s}^{-1})^2/\text{kpc}$  with a variance of  $17(\text{km s}^{-1})^2/\text{kpc}$  over the 9.2 to 13.4 Gyr interval at a radius 25 kpc. The monopole acceleration is radial and cannot create transverse velocities, although once present, non-radial velocities will vary as stars with the radial excursions of an orbit. The shape of the halo is slowly and somewhat erratically rotating, Fig. 4, with the eigenvalues of the quadrupole matrix fluctuating about 10% around their mean values. That is, the halo shows a semi-coherent vibration or ringing.

At fixed  $r$  the maximum tangential acceleration is  $a_z = \frac{3}{2}Q_1r$ , where  $Q_1$  is the largest eigenvalue of the

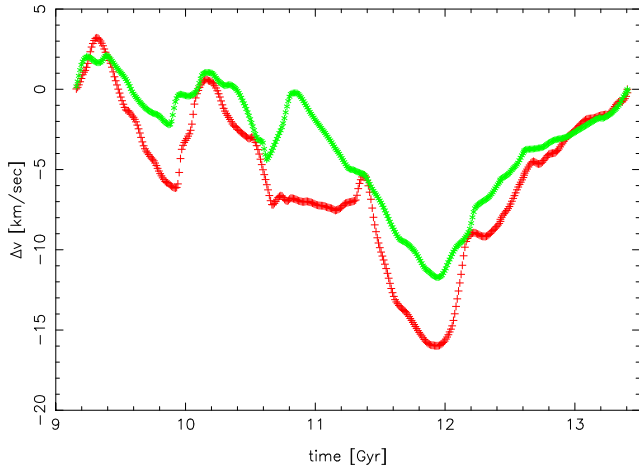


FIG. 6.— The variation in tangential velocity that the quadrupole moment can induce with time, calculated as the time integral of the accelerations in Figure 5 with the mean set to zero. Red is the analysis for 25 kpc potentials and green for 32 kpc. The calculation is done with a zero mean force over the interval.

quadrupole. Values of  $Q_1 r$  (without the  $\frac{3}{2}$ ) are plotted in Figure 5. At 25 kpc the quadrupole term  $Q_1 r$  has a mean and variance of 159 and  $12(\text{km s}^{-1})^2/\text{kpc}$ , respectively, with a range from  $121 - 217(\text{km s}^{-1})^2/\text{kpc}$  over the 4.5 Gyr interval analyzed. To estimate the scale of the velocities that can be induced perpendicular to an orbit the time variable component of the vertical acceleration is integrated over time,

$$\Delta v(t, r) = \frac{3}{2} r \int_{t_0}^t [Q_1(t', r) - \langle Q_1(r) \rangle] dt', \quad (2)$$

where  $\langle Q_1(r) \rangle$  is the average of the eigenvalue over the time interval. The fluctuating velocity change integral, Equation 2, leads to the values shown in Figure 6, demonstrating that the time variations of the quadrupole potential can create transverse velocities of  $10\text{-}20 \text{ km s}^{-1}$ . Such velocities would rise and fall with inward and outward excursions of the orbit. The dipole term has a mean and variance of 13 and  $5(\text{km s}^{-1})^2/\text{kpc}$ , respectively and is not dynamically very important, as expected deep in a halo.

The conclusion is that the semi-coherent fluctuations of the quadrupole leads to accelerations that produce velocities sufficient to cause the observed tangential velocities

of the streams. The variation can be characterized as a vibration or a strongly damped ringing oscillation.

#### 4. DISCUSSION AND CONCLUSIONS

The Orphan Stream is observed to have velocities incommensurate with the path of the stream. That is, there are significant transverse velocities. The implication is that the streams are in a time varying halo potential. This paper shows that ongoing late time accretion of dark matter sub-halos into the Milky Way-like galactic halo of the VL2 simulation leads to quadrupole potential fluctuations which can induce the transverse velocities in the  $10\text{-}20 \text{ km s}^{-1}$  range that the star streams in the simulation are measured to have. No doubt the presence of the LMC near to the Orphan Stream also contributes to the acceleration, and the LMC is being accreted onto the Milky Way, but the vibration of the dark matter halo is an ongoing activity. As more velocity measurements are acquired for streams in other locations around the galaxy it will be possible to separate an LMC force from the quadrupole ringing of the galactic halo, where the LMC force will be smaller further away, but the quadrupole induces the same accelerations on the other side of the galaxy.

Halo ringing is damped through the collisionless mixing of the accreted dark matter into the halo of the galaxy although significant substructure continues to circulate. If the dark matter self-interacts with a cross-section that leads to a mean free path,  $\ell$ , in the range of tens of kiloparsecs, then kinetic theory gives the kinematic viscosity as  $\nu \simeq \sigma_v \ell$ , where  $\sigma_v$  is the one-dimensional velocity dispersion of the dark matter. Viscosity transports momentum and will increase damping, potentially to a level that would largely suppress the halo vibrations. Self-interacting dark matter simulations can quantify the importance of the effect. If the Milky Way halo does not have the level of halo ringing expected for ongoing late time accretion it would provide a limit on the size of the dark matter self-interaction cross-section, with a quantitative result requiring simulations including self-interacting dark matter.

This research was supported by NSERC of Canada.

#### REFERENCES

- Belokurov, V., Evans, N. W., Irwin, M. J., et al. 2007, *ApJ*, 658, 337
- Bovy, J. 2015, *ApJS*, 216, 29
- Binney, J. 2008, *MNRAS*, 386, L47
- Carlberg, R. G. 2018, *ApJ*, 861, 69
- Carlberg, R. G. 2018, arXiv:1811.10084
- Carrillo, I., Minchev, I., Kordopatis, G., et al. 2018, *MNRAS*, 475, 2679
- Darling, K., & Widrow, L. M. 2019, *MNRAS*, 484, 1050
- Erkal, D., Belokurov, V., Laporte, C. F. P., et al. 2018, arXiv:1812.08192
- Eyre, A., & Binney, J. 2009, *MNRAS*, 400, 548
- Gaia Collaboration, Prusti, T., de Bruijne, J. H. J., et al. 2016, *A&A*, 595, A1
- Gaia Collaboration, Brown, A. G. A., Vallenari, A., et al. 2018, *A&A*, 616, A1
- Harvey, D., Revaz, Y., Robertson, A., & Hausammann, L. 2018, *MNRAS*, 481, L89
- Koposov, S. E., Belokurov, V., Li, T. S., et al. 2018, arXiv:1812.08172
- Madau, P., Diemand, J., & Kuhlen, M. 2008, *ApJ*, 679, 1260-1271
- Navarro, J. F., Frenk, C. S., & White, S. D. M. 1997, *ApJ*, 490, 493
- Newberg, H. J., Willett, B. A., Yanny, B., & Xu, Y. 2010, *ApJ*, 711, 32
- Pontzen, A., Roškar, R., Stinson, G., & Woods, R. 2013, *Astrophysics Source Code Library*, ascl:1305.002
- Read, J. I., Walker, M. G., & Steger, P. 2019, *MNRAS*, 488, 1813
- Sanders, J. L., & Binney, J. 2013, *MNRAS*, 433, 1813
- Spergel, D. N., & Steinhardt, P. J. 2000, *Physical Review Letters*, 84, 3760